Proceedings of the ASME 2020
Internal Combustion Engine Division Fall Technical Conference
ICEF2020
November 1-4, 2020, Denver, CO, USA

ICEF2020-2940

SIMULATIONS OF MULTI-MODE COMBUSTION REGIMES REALIZABLE IN A GASOLINE DIRECT INJECTION ENGINE

Sayop Kim[1], Riccardo Scarcelli[1], Yunchao Wu[2], Johannes Rohwer[1], Ashish Shah[1], Toby Rockstroh[1], and Tianfeng Lu[2]

[1]Argonne National Laboratory, Lemont, IL, USA
[2]University of Connecticut, Storrs, CT, USA

ABSTRACT

Lean and dilute gasoline compression ignition (GCI) operation in spark ignition (SI) engines are an attractive strategy to attain high fuel efficiency and low NOx levels. However, this combustion mode is often limited to low-load engine conditions due to the challenges associated with autoignition controllability. In order to overcome this constrained, multi-mode (MM) operating strategies, consisting of advanced compression ignition (ACI) at low load and conventional SI at high load, have been proposed. In this 3-D CFD study the concept of multi-mode combustion using two RON98 gasoline fuel blends in a gasoline direct injection (GDI) engine were explored. To cover the varying engine load demands, the combustion behavior in ACI and SI combustion mode was characterized and validated against experimental data. In order to evaluate part-load and transition between SI and ACI combustion, a mixed-mode combustion strategy was then explored numerically by creating a virtual test condition. The results of the mixed-mode simulations highlighted the conventional deflagrative flame propagation in SI mode transitioning to ignition-assisted end-gas autoignition. It was therefore deduced that the employed combustion model could reproduce the entire range of engine loads that multi-mode combustion would ultimately target.

Keywords: Multi-Mode Engine, SI, ACI, Mixed-Mode, G-Equation, Auto-Ignition, Wall-temperature sensitivity

INTRODUCTION

Gasoline engine can be operated under the condition of low-temperature combustion (LTC) regime in order to benefit from the greater thermal efficiency. Such an advanced compression ignition (ACI) strategy has been widely examined to demonstrate its diesel-like efficiency while emitting low levels of nitric oxides (NOx) and particulate matter (PM) [1, 2]. However, challenges associated with controlling autoignition in ACI mode may limit their use in low- or part-load conditions [3, 4].

Multi-mode (MM) combustion strategies have been shown to meet the operating range demands for SI engine platforms [5, 6, 7]. This type of strategy involves two distinctive combustion modes enabling engines to operate by selectively implementing high-load spark-ignition (SI) and low- and part-load advanced compression-ignition (ACI) at varying runtime engine-load demands. A key challenge to achieve multi-mode combustion is to enable mode-switching between ACI and SI and to ensure controlled autoignition. This mode transition should then be optimized in order to retain their inherent gains of each combustion mode.

Effective mode transition (e.g., ACI to SI or SI to ACI) is made possible by utilizing mixed-mode combustion consisting of flame propagation and controlled end-gas autoignition. Major bottleneck to this approach is associated with uncertainties in fuel-specific physiochemical behaviors such as auto-ignition, flame propagation and knock resistance Mixed-mode combustion has been investigated in numerous studies [8, 9, 10, 11]. Zigler and co-workers [8] investigated fundamental properties of ignition assisted by spark ignition in an optical research engine. Sjöberg and co-workers have studied lean gasoline mixed-mode combustion extensively [10, 12]. They highlighted substantial improvements in fuel economy for lean SI operation with the use of low octane gasoline, which effectively facilitates end-gas autoignition. This end-gas autoignition assists in completing the combustion event, which otherwise is inherently slow process in lean gasoline SI combustion.

Computational fluid dynamics (CFD) is capable of providing an effective tool to investigate key physics, often

undiscovered in experimental studies. Relatively few CFD activities on mixed-mode have been published to date. Middleton and co-workers [12] proposed a hybrid model that combines the Coherent Flamelet Model (CF) and detailed chemistry solver coupled with Multi-Zone (MZ) approach, named the CFMZ model to capture the premixed flame propagation followed by the end-gas autoignition process. Pal et al. [13, 14] proposed a novel hybrid combustion model to effectively reduce the computational time. In their hybrid model approach, the premixed flame front is captured by a level-set based G-equation model. This approach avoids the necessity of solving detailed chemistry in tracking the premixed flame front; hence it can dramatically reduce the computational load.

The first objective of this study is to discover important physics governing each of the combustion modes with respect to the turbulent mixing and ignition processes. The wall-temperature sensitivity presented in a previous study by the authors [15] is revisited in a more quantitative fashion. The second objective of this study is to discuss the feasibility of mixed-mode combustion as a mode transition strategy. To this end, a spark ignition assisted ACI (SACI) condition was numerically studied using the existing engine platform. Important insights into the mixed-mode combustion obtained from the SACI simulation are then discussed.

MATERIALS AND METHODS

In this study, 3-D full engine open cycle simulations were performed and validated against experiments. The experiments were conducted to achieve representative ACI and SI conditions only; mixed-mode combustion has yet to be tested experimentally. Details of experimental and CFD strategies are summarized in the following sections.

1 Engine Configuration and Test Conditions: ACI/SI

The experimental activities were performed on a single cylinder GDI engine at Argonne National Laboratory (ANL) which has been described in previous studies [16, 17, 18]. For ACI operation, the engine was equipped with a high compression ratio piston, but otherwise the standard GDI engine setup was retained. A Motec M800 engine control unit was used to control the injection timing and the fueling rate. Intake air was supplied by an Atlas Copco compressor and throttling was achieved by using a Parker Pilot regulator upstream of the intake manifold. To enable ACI mode, an electric intake air heater was used to maintain constant intake charge temperatures. Low speed engine and test cell data, such as the intake temperature and pressure, were logged at a sampling rate of 1 Hz using an in-house LabView based data acquisition system. Pertinent engine specification for ACI and SI conditions and their operating parameters are summarized in Table 1.

2 Numerical Simulation Setup

A commercially available CFD tool package, CONVERGE (v2.4.20) [19], was used to perform full open-cycle simulations

Table 1. *Engine specification and operating conditions for ACI and SI combustion*

Combustion chamber	Four valves, 40° pent-roof
Bore [mm]	89.04
Stroke [mm]	100.6
Compression ratio	15.3:1 / 12.7:1 (ACI/SI)
IVO / IVC [CA bTDC]	386 / 135
EVO / EVC [CA aTDC]	135 / 378
GDI injector	6-hole, solenoid
Co-Optima core fuel [RON / MON]	Alkylate [98.0/96.6] & E30 [97.4 / 86.6]
SOI [CA bTDC]	296
Engine speed [rpm]	1500
Intake pressure, p_{int} [bar]	1.35~1.45 / 0.8 (ACI/SI)
Intake temperature, T_{int} [°C]	135 / 35 (ACI/SI)
Injection pressure [bar]	150
Spark timing for SI only [CAD bTDC]	11.7 (Alkylate) / 14.3 (E30)
Global excess air ratio, λ [-]	2.6, 3.6 / 1.0 (ACI/SI)

of multi-mode engine operations. The adopted computational domain representing the employed Argonne single cylinder engine geometry is depicted in Figure 1. A modified cut-cell Cartesian method that can facilitate automatic grid generation was utilized with base grid size of 4 mm. Computational cells are dynamically generated or removed in the domain as the piston and valves are in motion. In order to better resolve the small scale (i.e., sub-grid scale) flow motion such as turbulent boundary layer, fixed embedding cells sizing down to 0.5 mm were constantly held in regions where static finer grid resolution is required. Additional finer mesh embedding (0.125 ~ 0.25 mm) was added during the initial flame kernel growth for spark ignition process. In addition, the adaptive mesh refinement (AMR) automatically applies finer grids in regions where finer fluid structure becomes substantial on runtime basis; e.g., steep

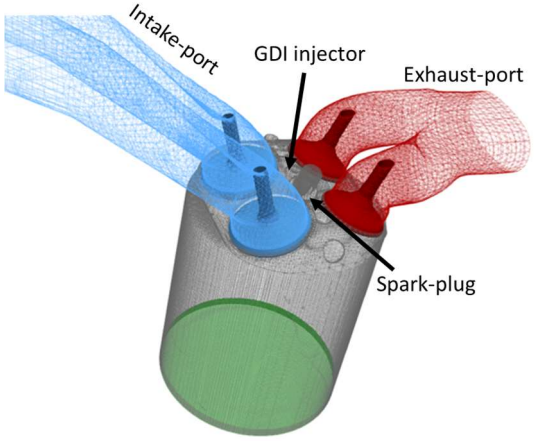

Figure 1*. 3-D CFD domain of the Argonne single cylinder engine with GDI injector and spark-plug mounted on cylinder head-center.*

gradient of reactive scalars and liquid spray particles are present. Minimum grid size of 0.5 mm was dynamically adopted in the region of such interests. The total cell count, in turn, reached the peak at 1.3 ~ 1.5 million during the simulation depending on the setup. The SI condition requires in general more cell counts due to finer grid resolution in the flame kernel region.

In-cylinder turbulent motion was modeled using the Reynolds-Averaged Navier-Stokes (RANS) solver with renormalized group (RNG) k-ε model with wall functions. To account for chemically reacting flow, the CONVERGE is integrated with SAGE detailed chemistry solver. This chemistry solver was then applied to address Well-Stirred Reactor (WSR) concept modeling in the RANS solver platform. The WSR model was also coupled with a Multi-Zone (MZ) [20] approach to further accelerate the computational speed. The MZ approach allows to group together similar computational cells and invoking the chemistry solver once per group. The number of zones is dynamically determined by specifying bin sizes. In this study, two dimensional bins were predetermined on equivalence ratio and mixture temperature spaces; 0.05 of equivalence ratio and 5 K of temperature. This combination of WSR-MZ setup was used to model spontaneous ignition of fuel-air mixture where small scale mixing is not dominant; i.e., well-mixed condition.

For turbulent premixed combustion encountered, a hybrid combustion modeling approach that has been recently proposed and validated across different SI engine platforms [21, 13] was used to capture SI and mixed-mode combustion. In this approach, level-set based flamelet model, G-equation model [22, 23], is employed to track the deflagration wave propagation initiated by spark ignition. This flamelet model allows to avoid solving stiff ODE calculations for chemistry in a thin reaction zone of premixed flame. The model is then to explicitly track the turbulent flame brush by a passive scalar transport, $G(\boldsymbol{x},t)$. This is enabled by resolving large scale motion of flame brush in turbulent flow, which is derived from the local turbulent flame speed (S_t) as a function of mixture properties, thermodynamics and turbulent intensity. The turbulent flame speed is calculated by the combination of laminar flame speed and small scale turbulent mixing contribution by following the Peters' formulation [22] of turbulent flame speed in correlation with predetermined laminar flame speed and local turbulent flow characteristics (Damköhler number, Da). The fuel-specific laminar flame speed was calculated on 1-D coordinate normal to a freely propagating premixed flame front *a priori*. Separate lookup tables for the laminar flame speed were then created as a function of temperature, pressure and equivalence ratio for currently employed fuels. This approach of tabulated laminar flame speed is therefore beneficial to incorporate fuel-specific effects on flame front motion.

In the current hybrid combustion model approach, burnt gas elements are treated as being in the equilibrium; therefore, stiff ordinary difference equation (ODE) calculation is not required. On the other hand, a separate WSR-MZ model approach is implemented to account for unburnt gas ($G < 0$); hence the fluid elements may undergo finite rate of chemical kinetics, requiring detailed chemistry solution. Validity of this hybrid model approach has been well demonstrated in knocking propensity of Cooperative Fuel Research (CFR) SI engine platform [13]. Details of model formulations and descriptions are not repeated in this paper for the sake of brevity. Additional details can be bound the Refs. [22, 23, 19, 13].

The gasoline fuel injection was modeled in an Eulerian-Lagrangian fashion. The clouds of liquid particles are treated in a Lagrangian coordinate and coupled with the continuous phase Eulerian solution. In order to address the spray atomization and evaporation process, Kelvin-Helmholtz (KH)-Rayleigh-Taylor (RT) breakup model [24] and Frossling correlation [25] were used, respectively. We adopted Co-Optima core research gasolines designed as part of the Co-Optima Initiative [26]. Two research gasolines, Alkylate and E30, were considered in this study. These fuels were formulated to obtain similar high Research Octane Number (RON), which is suitable for diluted/boosted SI operation. To treat these fuels in the liquid phase, the primary reference fuel (PRF97.3: iso-octane 97.3% and n-heptane 2.7% by volume) was substituted for Alkylate liquid surrogate. For the E30 liquid fuel blend, physical properties were referred to 30%-by-volume blend of ethanol with a certification gasoline that was generated in the previous literature [27].

For chemistry surrogate, on the other hand, 4 component blends for Alkylate and 8 components for E30 were suggested in the Co-Optima research initiative [26] to match their ignition characteristics with targeted research gasolines. The Table 2 shows details of their chemistry surrogate components. Chemical kinetics behavior of these two chemical surrogates were modeled by using two respective reduced mechanisms for Alkylate and E30; (1) 121 species and 647 reaction steps and (2) 211 species and 1239 reaction steps. The former mechanism (BOB-Alkylate) was developed by researchers at University of Connecticut and first introduced in the preceding ACI study [15]. The second mechanism was newly developed for BOB-E30 fuel in this study by the same kinetics group led by Lu. Details of the new mechanism developed is described in the following section.

Table 2. *Chemistry surrogate of Co-Optima research gasolines used in the investigation: Alkylate (ALK) and E30*

Co-Optima Gasoline	Chemistry component of fuel surrogate (by volume)
Alkylate (ALK)	iso-octane (93%), n-pentane (4%), n-butane (1%), 1,2,4-trimethyl-benzene (2%)
E30	iso-octane (26.6%), n-pentane (8.4%), n-butane (2.8%), 1,2,4-trimethyl-benzene (7.7%), n-heptane (11.9%), Hexene (4.9%), iso-pentane (7.7%), Ethanol (30%)

3 Development of Reduced Mechanism for Co-Optima Core Research Gasoline: E30

The chemical kinetics behavior of BOB-E30 was modeled using a 211-species skeletal mechanism for Co-Optima core research fuels, including BOB-Alk, BOB-Aro, and BOB-E30,

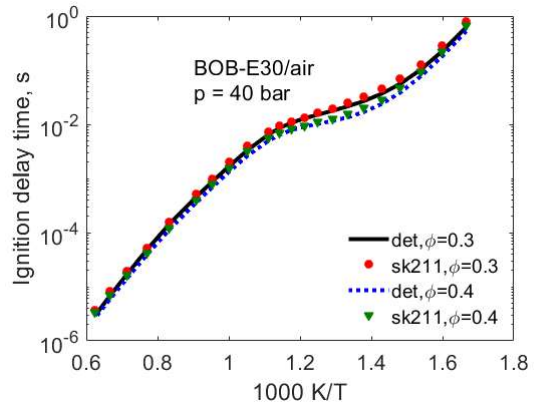

(a) Part-load ACI compatible condition

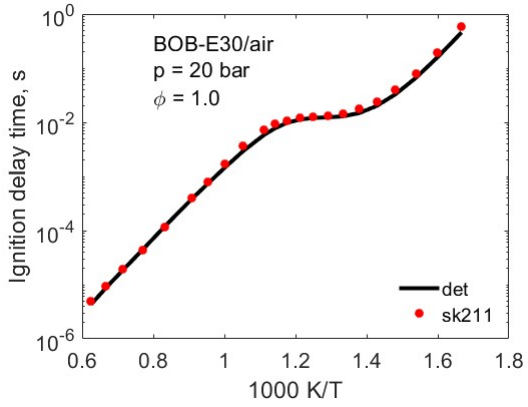

(b) High-load SI compatible condition

Figure 2. *A comparison of ignition delay times calculated using the detailed model (det) and the 211-species skeletal model (sk211) for BOB-E30/air mixtures aimed at multi-mode relevant conditions*

which is reduced from a 2878-species detailed mechanism for gasoline surrogates developed by the Lawrence Livermore National Laboratory (LLNL) [28]. The reduction was performed based on a large set of reaction states sampled over the parameter range of pressure from 1 to 100 atm, equivalence ratio from 0.3 to 1.5, inlet temperature of 700 K for perfectly stirred reactors (PSR), and initial temperature from 600 to 1600 K for auto-ignition, covering the low-temperature chemistry which is important for engine combustion. Due to the high efficiency, directed relation graph (DRG) was employed as the first step to reduce the large mechanism [29], with H radical selected as the starting species in DRG and the error tolerance was set to be 0.3. Then the DRG aided sensitivity analysis (DRGASA) [30] was applied to further eliminate unimportant species and reactions by specifying a worst-case relative error of 30% for ignition delay and extinction residence time in PSR, which is a quantification of the errors in the skeletal mechanism. The measured worst-case error tolerances for ignition delay and extinction residence time were 27.87% and 29.22%, respectively. The obtained skeletal mechanism is composed of 211 species and 1023 reaction steps.

The obtained 211-species skeletal mechanism is then validated against the detailed mechanism in evaluating the ignition delay times. The validation study was performed at multi-mode engine relevant conditions; lean-mixture and booting part-load ACI operation and stoichiometric SI operation. Selected validation results are displayed in Figure 2 (a,b) for mixtures of equivalence ratio of 0.3 and 0.4 under 40 bar and stoichiometric mixture under 20 bar respectively, showing close agreements between the 211-species skeletal mechanism and the detailed mechanism results.

RESULTS AND DISCUSSION

In this paper, primary results from the CFD analysis are organized by the representative engine conditions of multi-mode combustion in sequence of (1) ACI, (2) SI and finally (3) mixed-mode.

1 Advanced Compression Ignition (ACI) mode: low- or part-load conditions

This chapter continues to present further analysis of thermal wall-boundary condition impact that was not comprehensively discussed in the authors' preceding study [15] in a qualitative fashion. The authors carried out CFD simulations on several ACI conditions on the same engine platform ranging from low-loads (IMEP ~ 2 bar) to high-loads (IMEP ~ 9 bar). Important initial and boundary conditions were provided by the corresponding experimental data; e.g., intake charge thermodynamics and flow conditions. However the experiment lacks the thermal wall temperature condition on cylinder wall components; head, liner, valves and piston. Relevant approximation of temperature range of the walls were given based on a conjugated heat transfer (CHT) study [31] performed on a different SI engine platform for a range of engine loads considered in this study. Then, an empirical adjustment of temperature was applied to provide best agreement with the measured in-cylinder pressure trace. Hence, the wall temperature profile was defined by defining the follows: $T_{liner} = 425K$, $T_{piston} = 475K$, $T_{head} = 455K$, and $T_{valves} = 435K$. Given this boundary condition setup, majority of the model validation and important findings were discussed in the

Table 3. *Employed model validation against Argonne experiment: ACI mode with two Co-Optima research gasolines tested at one excess air ratio (λ=2.6) and intake temperature (T_{int}) of 135 °C.*

Fuels	Alkylate		E30	
	Exp.	CFD	Exp.	CFD
CA10	8.9	8.9	9.1	7.2
CA50	11.6	12.7	12.1	10.4
CA90	18.2	16.6	19.3	13.4
IMEP	6.5	6.8	6.0	6.5
COV_{imep}	1.3	0.7*	1.3	0.6*
P_{max}	69.1	67.5	62.5	67.1

(Unit: CA10-90 [deg.], COV_{imep} and P_{max} [bar], *under-valued COVimep is induced by RANS modeling feature.)

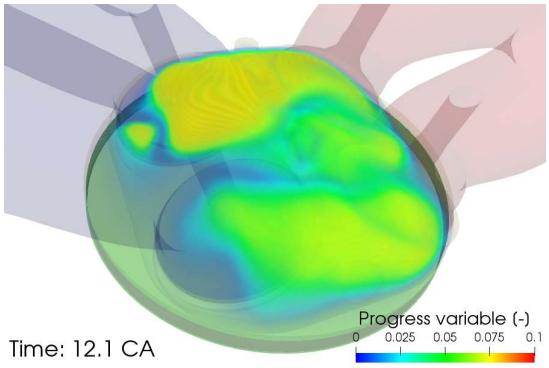

(a) Characteristics of ACI combustion: volumetric ignition occurs over the entire cylinder volume (progress variable defined as sum of mass fraction of CO and CO_2.

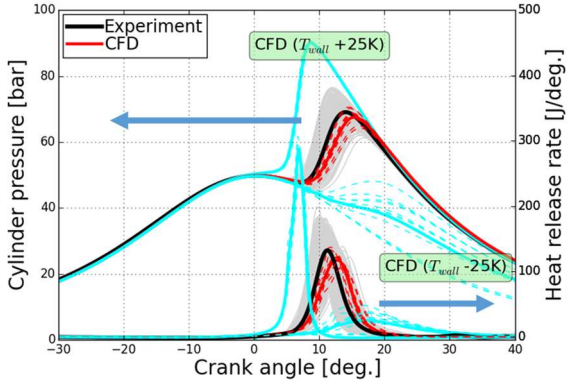

(b) Wall temperature sensitivity tested on Alkylate part-load (baseline) condition.

Figure 3. *Representative characteristics of ACI combustion event: (a) volumetric combustion and (b) substantial impact of wall temperature: Cyan curves indicate the impact of wall temperature perturbation on combustion phasing.*

preceding papers [15, 32]; hence short summary of engine performance metrics listed in Table 3 replaces baseline ACI simulations performed in the previous studies.

In ACI engine, major interests found in the authors' earlier studies [15, 32] were two-fold; i.e., (1) volumetric and spontaneous combustion event and (2) the cylinder wall temperature sensitivity as illustrated in Figure 3. As, indeed, "homogeneous" mixture charge is hardly achieved, the growth of progress variable (PV: Y_{co} + Y_{CO2}) accordingly proceeds in sequential process to a certain extent. Nonetheless, the Figure 3 (a) is better representative of such a volumetric burning process. Hence, the use of WSR-MZ model seems to be well suited. In addition, Numerical experiments in the authors' earlier study [15] revealed a certain level of wall temperature perturbation that substantially affects the combustion phasing and combustion stability. The numerical experiments applied 25*K* temperature perturbation applied across entire cylinder wall components and observed significant shift of pressure trace indicated by cyan curves in Figure 3 (b). However, the earlier study [15] did not yield quantitative clues on this observation. Hence, the present study put forth a question on this finding that can potentially be answered by exploring multi-variables joint analysis.

The previous studies [15, 32] identified certain degrees of sensitivity of mixture stratification and thermal stratification respectively in ACI engine combustion phasing. However, coupled impact of both type of stratification levels on ignition of local mixture element has not been comprehensively examined. To this end, this study proposes a novel method of analysis that can provide an illustrative measure of auto-ignition characteristics associated with mixture/thermal stratifications. In this new method of analysis, mass-weighted joint PDF in percentile of temperature and equivalence ratio (ϕ) is overlaid on an ignition delay time map (See Figure 4). The joint PDF was constructed by averaging mixture quantities over 5 consecutive cycles constantly at TDC timing where noticeable low-temperature reaction is yet to begin. For constructing the ignition time delay map, the pressure was held constant at 50 bar (mean

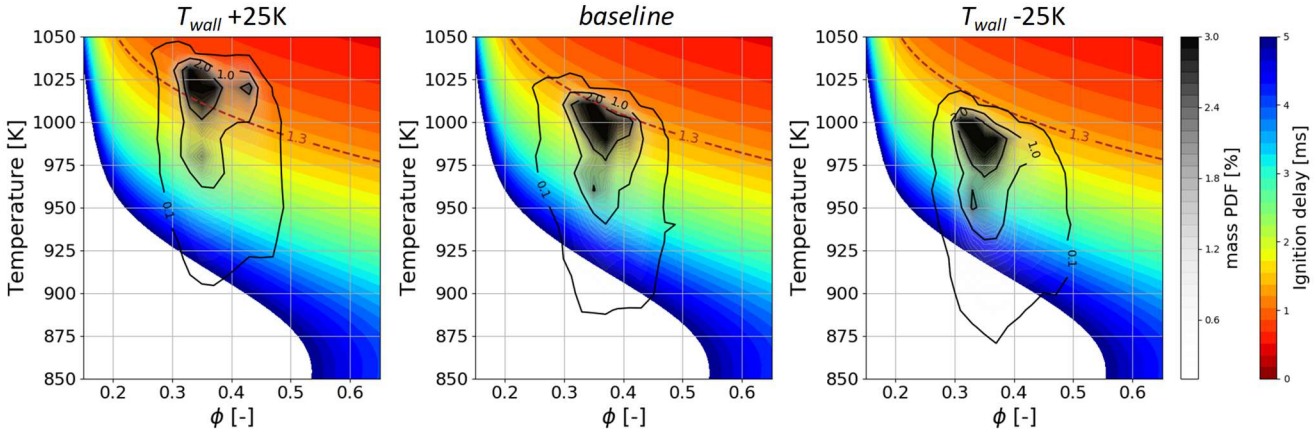

Figure 4. *Wall temperature sensitivity analysis on mixture reactivity map represented by static ignition delay time. Mass-weighted probability density function (mass PDF) is shown to represent the mixture and thermal stratification evaluated at top dead center (TDC) prior to substantial ignition event. The red dashed line (τ_{chem}=1.3 ms) represents the finite level of residence time from TDC to CA50.*

pressure at TDC) since the pressure would not hold as heavy impact as temperature and equivalence ratio would have on the ignition delay. In order to examine whether the mixture element of interest would proceed the high-temperature combustion at desired CA50 timing, a chemical time scale (τ_{chem}) was introduced to measure time elapsed from TDC to CA50; i.e., τ_{chem} ~ 1.3 ms at given engine operating condition (1500 rpm). Therefore, it is reasonable approximation that the mixture elements within the τ_{chem} limit can undergo high-temperature heat release prior to the designated CA50. This method of analysis can be applied in the discussion of wall temperature sensitivity.

Along with the given test data (baseline), two additional numerical tests were conducted by imposing thermal wall boundary condition with perturbations of 25K temperature; see Figures 3 and 4. In the baseline scenario presented in Figure 4, only a portion of the mixture elements comes within the chemical reactivity limit (1.3 ms). This portion of mixture quantity may have been responsible for the onset of high-temperature combustion prior to CA50 and transported thermal energy to the neighbor mixture elements, resulting in sequential burning process. This sequential burning process was quantitatively highlighted in the preceding study [32]. It is also noteworthy that wall temperature change by 25K level can noticeably shift the thermal quantity distribution of mixture while maintaining the non-uniformity of thermal mixture relatively constant in its PDF shape. In consequence, majority of the mixture charge mass with +25K wall temperature scenario is found to fall within the time scale (τ_{chem}) limit and hence resulting in explosively fast reaction process. In contrast, -25K wall temperature case forces the majority of mixture to be chemically inert and fail to meet desired combustion phasing.

On this map, one can see higher degree of reactivity change in temperature space given the equivalence ratio range of interest ($0.25 < \phi < 0.5$), meaning that the employed ACI conditions were operated in the domain of very temperature sensitive region. Conversely, mixture charge stratification in ϕ may have imposed a less influential impact. This is very consistent tendency of *T*-ϕ sensitivity with observations in the previous study [15].

2 Spark Ignition (SI) mode: high-load stoichiometric condition

The hybrid combustion model approach for SI mode combustion is first validated against the experiments in this section. Corresponding engine experiments were performed aiming to produce high-load SI engine conditions (IMEP ~ 9 bar) with stoichiometric mixture charge. Two different Co-Optima research gasolines were used to highlight the robustness of the model accuracy and validity. With these two different fuels used, the model empirical constants were not found case-dependent; namely ensuring the robustness of the model setup. Calculated pressure and heat release traces for two fuels are also found to well follow the trend of experiment. Table 4 summarizes the key engine performance metrics evaluated by experiment and the current CFD approach for model validation purpose. Slightly mismatching combustion phasing in Figure 5 is possibly

Table 4. *Employed model validation against Argonne experiment: stoichiometric SI mode combustion with two Co-Optima research gasolines and intake temperature (T_{int}) of 35 °C. Chamber wall temperature adjusted in wall component basis: T_{liner} = 490K, T_{piston}=540K, and T_{head}=520K*

Fuels	Alkylate		E30	
	Exp.	CFD	Exp.	CFD
CA10	5.7	5.5	3.5	4.9
CA50	19.2	18.3	15.4	18.7
CA90	30.4	36.9	26.0	34.4
IMEP	8.9	8.7	9.0	9.0
COV_{imep}	2.9	2.2*	2.6	1.9*
P_{max}	40.3	39.3	44.8	39.0

(Unit: CA10-90 [deg.], COV_{imep} and P_{max} [bar], *under-valued COVimep is induced by RANS modeling feature.)

attributed to the use of simplified ignition kernel growth modeling during the energizing stage. Indeed, to avoid numerical complexity and intense time integration in the ignition modeling, we utilized a simple approach to mimic the ignition kernel formation and growth by imposing an energy source at the spark plug location.

To feature the cyclic engine operations, 11 consecutive open-cycles were collected at each test condition. The 1st cycle was then discarded to reduce the initialization artifacts and the remaining 10 cycles were used for analysis. The current RANS modeling framework did not capture higher bandwidth of pressure variance from cycle to cycle. This is indicated by unde-estimated COV_{imep} compared to measurement. This is primarily attributed to the fact that RANS framework tends to smooth out the numerical solution with ensemble averaged scalars and presence of turbulent viscosity term (i.e., Reynolds stress). Hence, small scale turbulent motion may disappear. However, large scale fluctuating fluid motion can be retained and attribute to the cyclic combustion dynamics. Earlier CFD researches [33, 34, 35] have demonstrated the relevance of using RANS framework in capturing qualitative trend of CCV impact. They addressed that RANS modeling can capture portion of the CCV events and reproduce generic trends of cyclic events.

Given the well validated baseline simulation, this section aims to discuss underlying principles governing the main features observable in high-loads SI mode. Figure 6 shows the results obtained from the wall temperature sensitivity analysis. As opposed to ACI mode, the SI mode features marginal influence of wall temperature on key combustion metrics; i.e., IMEP, and combustion phasing. While the ACI mode was hugely affected by only a 25K difference in T_{wall}, up to 65K difference in T_{wall} barely makes change in presented combustion metrics in Figure 6. It only appears to merely affect the combustion phasing in a small range of 3 CAD, which is very small change compared to that of ACI mode condition. It is logically true that thermal wall boundary condition would not affect the major source of SI combustion event; rather the energy deposition in spark plug and subsequent flame kernel growth would be more influential.

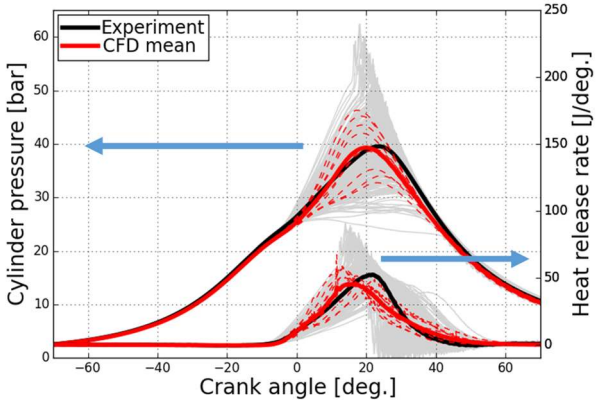

(a) Fuel: Alkylate (Spark timing: 11.7 CAD bTDC)

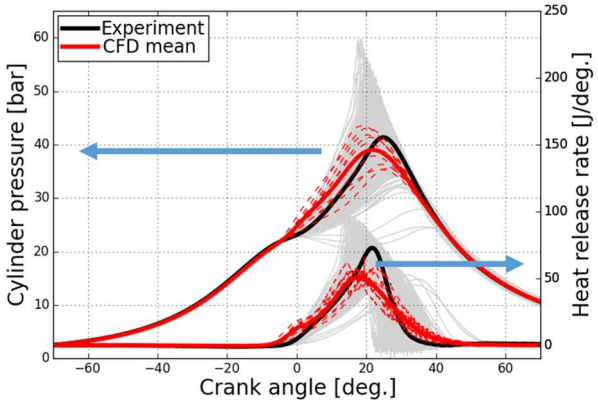

(b) Fuel: E30 (Spark timing: 14.3 CAD bTDC)

Figure 5. *Validated simulations with use of combustion model (G-equation/WSR-MZ) compared to Argonne stoichiometric SI combustion.*

One of the prominent features of the SI can be noticed by the enlarged cycle-to-cycle (CCV) variation in both experiment and simulation. The SI mode almost doubles the CCV impact compared to that of ACI mode. Since the SI combustion features premixed flame propagation, possible sources of the CCV can be found from local variations in (1) mixture thermodynamic state and (2) fluid dynamics. Following discussions explores the CCV impact in these two aspect.

From aspect of the thermodynamic state, potential source of CCV in SI mode may stem from the cyclic/spatial variability of thermal-mixture element. This, in turn, changes the local laminar flame speed. In this context, the same fashion of analysis introduced in Figure 4 is applied to the SI mode. Instead of using ignition delay map, we used a map of laminar flame speed (LFS) as a function of temperature and pressure as displayed in Figure 7. The thermal-mixture stratification is apparent as represented by the joint PDF of equivalence ratio and temperature. The mixture elements may feature varying laminar flame speed in association with the joint PDF. From this map, one can roughly spot the LFS values ranging 0.6 ~ 0.8 m/s (green to yellow on

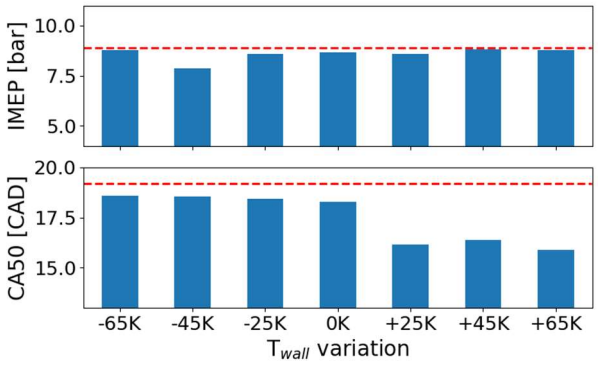

Figure 6. *Wall temperature (T_{wall}) sensitivity on combustion metrics in the high-load SI operation. This numerical experiment was conducted with the baseline setup (Alkylate). Red dashed line indicate the measured level from the experiment.*

the color map) to best represent dominant mixture thermodynamic property. This is too slow speed for the flame front to travel through half of the bore dimension (44.5 mm) within the effective duration of combustion event (50 deg. equivalent to 5.5 ms). The flame front may require around 55.5 ms in order to travel through the combustion chamber (10 times the engine combustion period). In other words, laminar flame speed contributes marginal impact to flame-travel-through-time in combustion chamber. When it comes to the CCV impact, the impact of static thermodynamic variation (laminar chemistry) on CCV tendency could be rather outweighed by the fluid dynamics impact.

From a different aspect, the increased CCV level may be attributed to in-cylinder fluid dynamics in different length scale. In the current simulations, large scale motion (e.g., tumble flow) induced by intake charge is considered identical across different cycles since cyclic average of intake flow was imposed at the intake manifold boundary condition. Indeed, it is reasonable approximation because the experiment did not identify significant cyclic perturbation in the intake port charge flow condition. Hence, primary characteristics of cyclic combustion event in the SI engine may be attributed to the interaction between flame front and small scale turbulent mixing. In this context, underlying characteristics of CCV event can be understood in conjunction with the local turbulent mixing intensity. Illustrated graphics in Figure 8 well represent this scenario; two-fold end-cycle bands (weak/strong cycles: lower-end and upper-end) are selected to compare the turbulent intensity and consequence of flame front propagation. The figures seem to explain the strong correlation of combustion cycle and local turbulent intensity. Further analysis shown in Figure 9 supports this idea. We gathered three representative cycles of upper-end, lower-end and median cycle. The burnt gas in Figure 9 (a) is measured by the ratio of burnt gas mass over the total gas mixture; thereby standing for the progress rate of turbulent flame brush. Figure 9 (b) quantifies the intensity of turbulent mixing filtered at flame front (captured within -0.001 < G <0) and accordingly tracks the temporal history of the

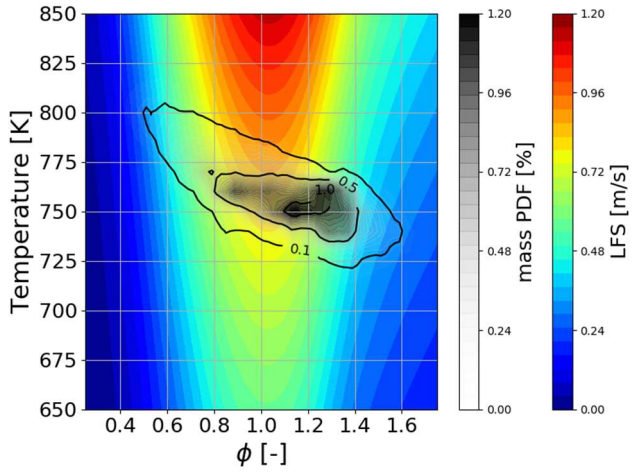

***Figure 7**. Mass-weighted probability density functions (PDFs) of equivalence ratio and temperature overlaid on the laminar flame speed (LFS) map. LFSs were evaluated by solving 1-D freely propagating laminar flame using CONVERGE detailed chemistry solver.*

mixing intensity. This suggests strong positive correlation between turbulence intensity and flame propagation speed.

This turbulence impact on the CCV is fairly well-known physics in normal SI engine operations and has been discovered in many literatures [36, 37, 38]. Nonetheless, this study attempts to gain understanding of contribution of turbulent intensity competing with laminar state thermal-mixture charge. Additional numerical experiments were performed for the three given cycles at following conditions: (1) laminarized flame and (2) imposed homogeneous turbulence. The first test, laminarized flame scenario, forces the flame to undergo laminar flame propagation without an impact of turbulence. This was simply done by turning off the turbulent flame speed (S_t) contribution to transport of the level-set G scalar. Shown result in Figure 9 (a) suggests that the contribution by the pure laminar flame speed impact is minimal. Only 1% of unburnt gas was swept by the laminarized flame till 40 CAD aTDC. Due to the intrinsic nature of LFS, the difference between three cycles seems to be attributed to the impact of thermal-mixture charge stratification evaluated in Figure 7.

The second test is to evaluate the contribution from the thermal-mixture state variability to the CCV. The homogeneous turbulence field was artificially imposed identically to the three cycles, such that cyclic variability of turbulence flow impact is removed. Mean turbulent kinetic energy (TKE) and energy dissipation rate (EPS) values were extracted from the median cycle at 12 CAD bTDC shortly before the spark timing and imposed to these three cycle simulations at the same time. In order to neglect the production of turbulence by the large scale motion, convective velocity components were also reinitialized with zero values; i.e., u=v=w=0. Strictly speaking, from energy balance stand point, the flow field becomes non-stationary and decaying turbulent flow (i.e., no production of turbulence). This feature is evident by finding the monotonously decaying TKE trajectory filtered at flame front as illustrated in Figure 9 (b). Under this circumstance, the impact of turbulence is retained equally across the three different cycles; hence other competing impact (thermal-mixture state variation) becomes effective. In the result seen in Figure 9 (a), cyclic variation of burnt gas is still present. Therefore, it can be claimed that a part of CCV source comes from the cyclic variation of local thermal-mixture charge.

3 Mixed-Mode Combustion: ignition-assisted ACI combustion with lean mixture

The validity of the employed combustion model holds true by sweeping the two-end modes of multi-mode combustion; low-load ACI and high-load SI. Hence, it is also a reasonable approach to apply the consistent model setup to produce the part-load mixed-mode combustion regime in the same Argonne engine platform. In this section, the mixed-mode combustion is

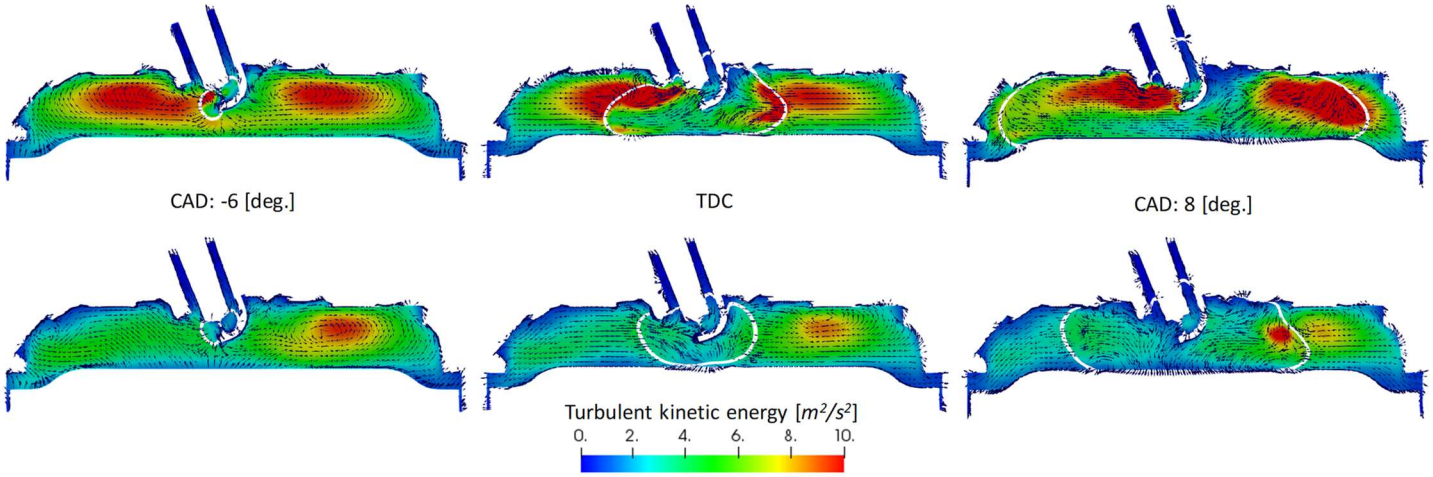

***Figure 8**. Cycle-to-cycle variability (CCV) captured in turbulent flame front: Two different cycles that make CCV bandwidth are chosen to present: (upper) high-end cycle (lower) lower-end cycle. White solid line indicates the turbulent flame front identified at G = 0. Colored contour map features turbulent intensity.*

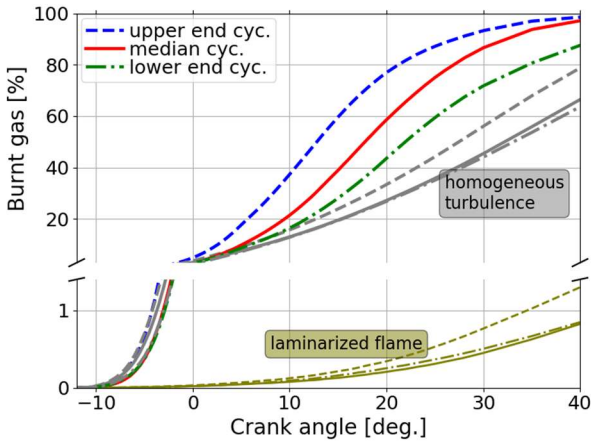

(a) Turbulent flame brush progress rate represented by burnt gas ratio.

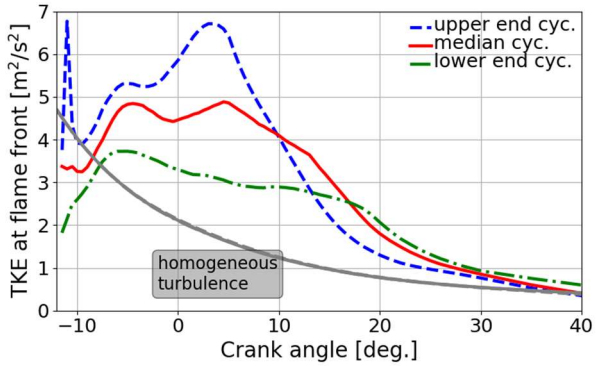

(b) Turbulent flame front filtered turbulent kinetic energy

***Figure 9**. Impact of turbulent intensity on turbulent flame brush progress and two different numerical experiments: test (1) laminarized flame and test (2) homogeneous turbulence.*

taken as a strategy for mode transition between ACI and SI; hence both distinctive combustion modes likely coexist in the transitional mode operation. However, the mixed-mode combustion has yet to experimentally be attempted in the currently employed engine platform; no available experimental data exist to this date. Therefore, following discussions are to highlight numerically explored important physics observed mixed-mode combustion.

Towards the goal of mixed-mode combustion strategy using the consistent engine platform, we created a virtual test condition for mixed-mode while maintaining the same engine dimensions with the ACI and SI operations. . The virtual test condition was intended to benchmark the major engine parametric features used in the published mixed-mode combustion studies [9, 21]. The benchmarked engine was featured of direct injection spark ignition (DISI) and explored to realize the spark ignition assisted ACI (SACI) operation. Important engine parametric features used for the virtual test are listed in Table 5.

Figure 10 (a) shows the pressure and heat release rate traces obtained from a single simulation at the virtual test condition. Although no direct experimental data is available for validation purpose, the current simulated condition apparently captures an evidence of finding mixed-mode combustion feature. This evidence of mixed-mode combustion propensity was similarly repeated in the previous study [21]. The currently simulated engine load (IMEP) yields 4.6 bar, which is very close to the benchmarked experiment, 4.46 bar.

Coordinate transform of heat release rate trace can additionally highlight distinctive feature of mixed-mode combustion regimes. In Figure 10 (b), the mass burned rate replaces the crank angle coordinate. The burned mass fraction was calculated as the integrated heat release rate normalized by total heat release at each cycle. In this feature, first rise of heat release is constantly observed over entire cycles; however second rise at different rate from cycle to cycle is featured at a later phase, here around 80% of mass burned rate, which is very close to the measured rate in the experiment [9]. The presence of the second heat release peak gives a clever way to systematically distinguish the 'mixed' two combustion regimes. It is apparent that the SI initiated flame front propagation features first rise of heat release; therefore the second peak suggests an indication of assisted auto-ignition, namely spark ignition-assisted ACI (SACI). However, a portion of captured cycles was observed to skip the second peak of heat release as indicated in blue solid lines. This study is therefore intended to primarily reveal the governing physics behind these distinguished combustion behaviors.

Time sequence of flame structures for two different combustion regimes is illustrated in Figure 11; upper row with mixed-mode and lower row with SI-only mode. These distinguishable combustion event can be clarified by the evidence of spontaneous ignition of unburnt gas. The mixed-mode combustion shown here, sequential event of SI initiated deflagration wave and subsequent end-gas auto-ignition, can also be distinguished by apparently fast flame front progress rate indicated by blue color iso-surface. Therefore, it can be hypothesized that the fast burning flame front pushes the end-gas mass towards cylinder wall. This may result in accelerating the end-gas heating and spontaneous combustion.

***Table 5.** Virtual Argonne single cylinder engine test condition for reproducing mixed-mode combustion*

Compression ratio	12:1
GDI injector	6-hole, head-center mounted
Co-Optima core fuel [RON / MON]	E30 [97.4 / 86.6]
SOI [CA bTDC]	300
Engine speed [rpm]	1500
Intake pressure, p_{int} [bar]	0.85
Intake temperature, T_{int} [°C]	100
Injection pressure [bar]	150
Spark timing	57 CAD bTDC
Global excess air ratio, λ [-]	1.75

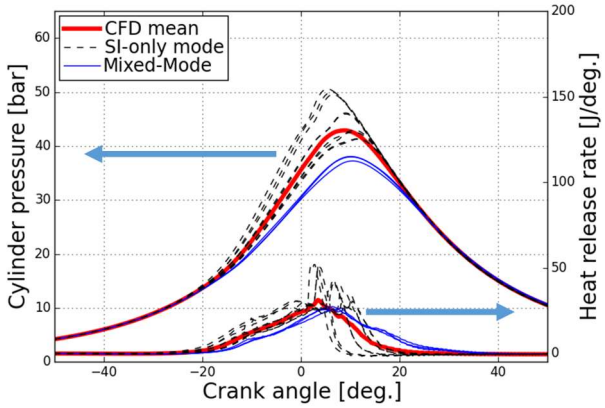

(a) Pressure and temperature heat release

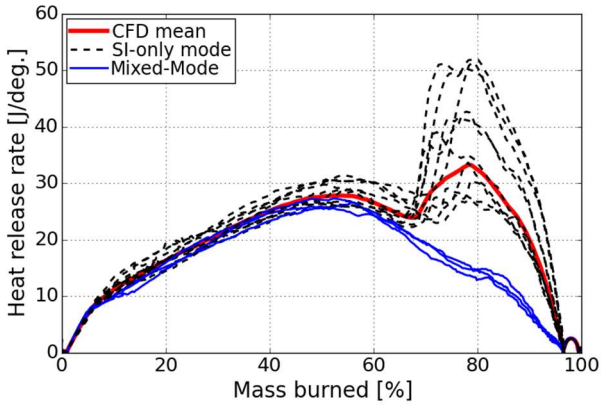

(b) Heat release rate in burned mass fraction space

Figure 10. *Virtually tested mixed-mode combustion reproduced at Argonne single cylinder engine platform (13 cycles obtained and averaged)*

It should be noted that the mechanism of the mixed-mode is very similar to the one behind the knocking propensity. The mixed-mode excludes abnormal rise of pressure; otherwise this scenario would become knocking phenomena. Therefore, a method of analysis on end-gas reactivity that has been popularly utilized by the preceding literatures [39, 40, 41] can also be used. In this context, pressure and temperature trajectory of the end-gas phase ($G < 0$) was captured after spark timing and displayed on the fuel-specific (E30 in this test) static ignition delay time. Symbols in Figure 12 mark sample points of CADs along the trajectory; hence one can see the progress rate of end-gas compression. Aforementioned hypothesis holds in this analysis of P-T trajectory. The mixed-mode is appeared to be promoted by the accelerated end-gas pressure rise by the flame front, whereas the SI-only mode failed to rise up to a certain state of thermodynamic that can initiate high-temperature kinetics.

It is now noted that the flame front progress rate is responsible for identifiable mixed-mode. Therefore, the insight gained from the SI combustion mode also holds valid in the mixed-mode and allow to derive informative understandings. From this perspective, result shown in Figure 13 accounts for contribution of turbulent mixing at the flame front to the burnt gas progress rate. This derives a solid implication that the mixed-mode cycles were consistently accompanied by increased level of turbulent mixing at the flame front which in turn augmented progress rate of the SI (deflagration wave) mode. In a general notion, auto-ignition is kinetically driven; hence chemically reactive fuels (e.g., low RON#) may be more compatible with mixed-mode repeatability. However, findings in this section suggest that turbulent mixing can also assist the end-gas auto-ignition to enhance the mixed-mode combustion potentially with high RON fuels.

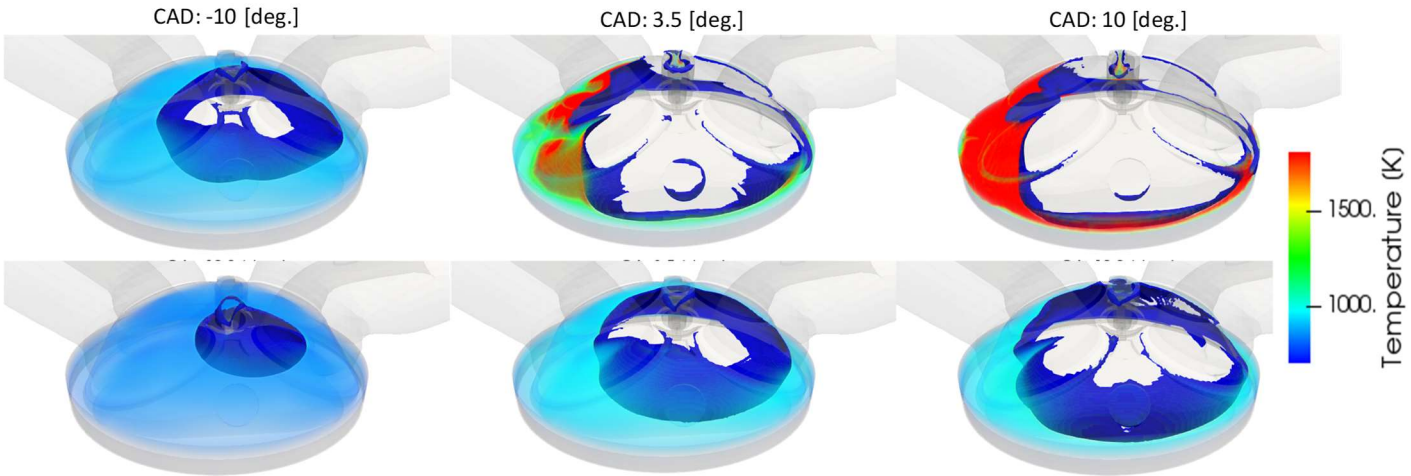

Figure 11. *Two distinctive cyclic features of mixed-mode combustion: (upper) mixed-mode combustion realized, (lower) deflagration wave (SI) only observed. The deflagration (spark ignition initiated flame front) is identified by blue colored iso-surface (G=0). The end-gas thermodynamic state is featured by temperature. A sudden increase of temperature indicates auto-ignition of end-gas mixture.*

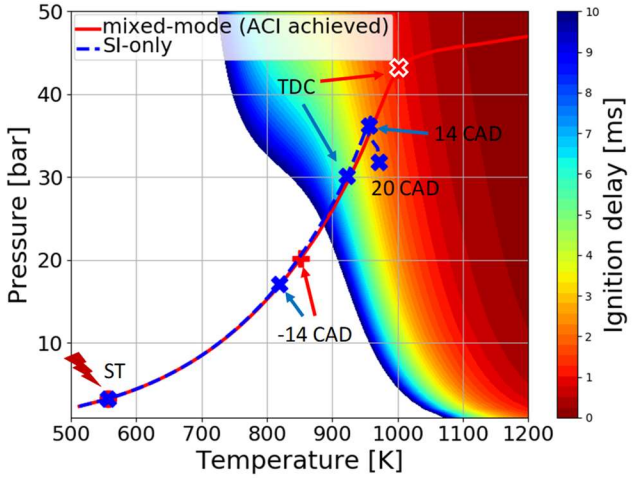

***Figure 12**. Pressure-Temperature trajectories of end-gas mixture for two distinguished combustion regimes observed in mixed-mode combustion*

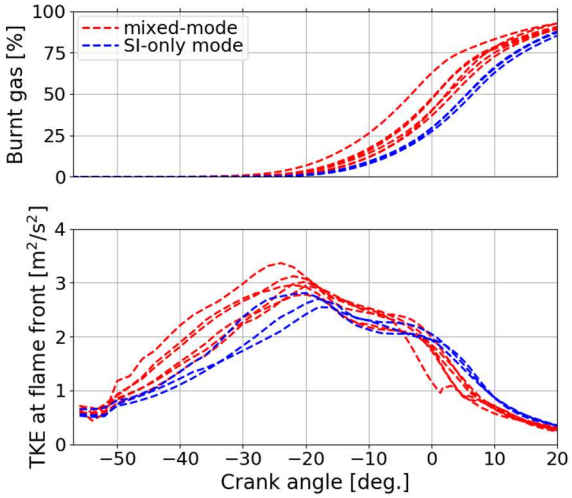

***Figure 13**. Impact of local turbulent intensity on cyclic-to-cycle varying mixed-mode combustion regimes*

CONCLUSION

Key outcome of this study is to show the model capability of simulating the realizable multi-mode combustion strategies and introduce novel method of analysis to understand in-depth physics. Key summaries are listed as follows:

1. In the ACI simulations, WSR-MZ model approach moderately captures the experimental trend and characterizes the volumetric combustion event. This approach also enables to provide parametric analysis with the wall temperature uncertainty. Such a wall temperature impact plays a role in determining the combustion phasing. This phase control can be greatly influenced by the chemical reactivity variation along with the stratified mixture charge.
2. Standard SI operations in the GDI engine were simulated with a recently proposed hybrid combustion model (level-set G-equation model with WSR-MZ approach). The model was useful to capture major features observed in the SI combustion revealed by the experiment.
3. Major source of CCV in SI operation stem from local turbulence intensity, which greatly affects the progress rate of premixed flame brush. A numerical experiment performed in this study created a cyclic constant homogeneous turbulent flow field. The test revealed a partial source of CCV stemming from the cyclic variation of thermal-mixture charge.
4. As a strategy of mode transition for multi-mode engines, this study discusses a mixed-mode operation that combines major features of ACI and SI operations. A virtual test condition was designed in order to reproduce the mixed-mode combustion that was demonstrated in a preceding experiment. The virtual test condition with the Argonne engine configuration replicated the same findings and consistent level of mixed-mode probability as seen in the previous experimental investigation.
5. The use of the hybrid combustion model was capable of providing insightful notions in terms of source of mixed-mode realization and impact of local turbulent mixing. From the result noted from the virtual test, elevated turbulence intensity can enhance the probability of mixed-mode combustion regime. This also suggests an potential use of high RON (low-reactivity) fuels in the mixed-mode combustion if increased turbulent mixing intensity is ensured near the spark plug location.

ACKNOWLEDGEMENTS

The submitted manuscript has been created in part by UChicago Argonne, LLC, Operator of Argonne National Laboratory (“Argonne”). Argonne, a U.S. Department of Energy Office of Science Laboratory, is operated under Contract No. DE-AC02-06CH11357. The U.S. Government retains for itself, and others acting on its behalf, a paid-up nonexclusive, irrevocable world- wide license in said article to reproduce, prepare derivative works, distribute copies to the public, and perform publicly and display publicly, by or on behalf of the Government. The Department of Energy will provide public access to these results of federally sponsored research in accordance with the DOE Public Access Plan. http://energy.gov/downloads/doe-public- access-plan. This work is performed under the auspices of the Office of Energy Efficiency and Renewable Energy, Office of Vehicle Technology, U.S. Department of Energy, as part of the Co-Optimization of Fuels & Engines (Co-Optima). Finally, the author thank the U.S. Department of Energy Vehicles Technology Office (technical manager: Kevin Stork) for financial support.

REFERENCES

[1] S. Ciatti, M. Johnson, B. Adhikary, R. Reitz and A. Knock, "Efficiency and Emissions Performance of Multizone Stratified Compression Ignition Using Different Octane Fuels," in *SAE Technical Paper 2013-01-0263*, 2013.

[2] V. Manente, B. Johansson and W. Cannella, "Gasoline Partially Premixed Combustion, the future of internal combustion engines?," *Int. J. Engine Research,* vol. 12, no. 3, pp. 194-298, 2011.

[3] S. Ciatti and S. N. Subramanian, "An Experimental Investigations of Low Octane Gasoline in Diesel Engine," *J. Eng. Gas Turb. Power,* vol. 133, p. 092802, 2011.

[4] C. P. Kolodziej, S. Ciatti, D. Vuilleumier, B. D. Adhikary and R. Reitz, "Extension of the Lower Limit of Gasoline Compression Ignition with 87 AKI Gasoline by Injection Timing and Pressure," in *SAE Technical Paper 2014-01-1302*, 2014.

[5] A. Kulzer, J.-P. Hathout, C. Sauer, R. Karrelmeyer, W. Fischer and A. Christ, "Multi-Mode Combustion Strategies with CAI for a GDI Engine," in *SAE Technical Paper 2007-01-0214*, 2007.

[6] G. Lavoie, J. Martz, M. Wooldridge and D. Assanis, "A multi-mode combustion diagram for spark assisted compression ignition," *Combustion and Flame,* vol. 157, pp. 1106-1110, 2010.

[7] S. Nüesch, A. Stefanopoulou, L. Jiang and J. Sterrniak, "Fuel Economy of a Multimode Combustion Engine With Three-Way Catalytic Converter," *Journal of Dynamic Systems, Measurement, and Control,* vol. 137, p. 051007, 2015.

[8] B. Zigler, P. Keros, K. Helleberg, M. Fatouraie, D. Assanis and M. Wooldridge, "An experimental investigation of the sensitivity of the ignition and combustion properties of a single-cylinder research engine to spark-assisted HCCI," *Int. J. Engine Res.,* vol. 12, no. 4, pp. 353-375, 2011.

[9] M. Sjöberg and W. Zeng, "Combined Effects of Fuel and Dilution Type on Efficiency Gains of Lean Well-Mixed DISI Engine Operation with Enhanced Ignition and Intake Heating for Enabling Mixed-Mode Combustion," *SAE Int. J. Engines, 9(2),* 2016.

[10] Z. Hu, J. Zhang, M. Sjöberg and W. Zeng, "The use of partial fuel stratification to enable stable ultra-lean deflagration-based spark-ignition engine operation with controlled end-gas autoignition of gasoline and E85," *Int. J. Engine Res.,* pp. 1-18, 2019.

[11] M. Sjöberg and X. He, "Combined effects of intake flow and spark-plug location on flame development, combustion stability and end-gas autoignition for lean spark-ignition engine operation using E30 fuel," *Int. J. Engine Res.,* vol. 19, no. 1, pp. 86-95, 2017.

[12] R. Middleton, L. Olesky, G. Lavoie, M. Wooldridge, D. Assanis and J. Martz, "The effect of spark timing and negative valve overlap on spark assisted compression ignition combustion heat release rate," *Proceedings of the Combustion Institute,* vol. 35, pp. 3117-3124, 2015.

[13] P. Pal, Y. Wu, T. Lu, S. Som, Y. See and A. Moine, "Multidimensional Numerical Simulations of Knocking Combustion in a Cooperative Fuel Research Engine," *J. Energy Resources Tech.,* vol. 140, p. 102205, 2018.

[14] P. Pal, C. Kolodziej, S. Choi, S. Som, A. Broatch, J. Gomez-Soriano, Y. Wu, T. Lu and Y. C. See, "Development of a Virtual CFR Engine Model for Knocking Combustion Analysis," *SAE Int. J. Engines,* vol. 11, pp. 1069-1082, 2018.

[15] S. Kim, J. Kim, A. Shah, P. Pal, R. Scarcelli, T. Rockstroh, S. Som, Y. Wu and T. Lu, "Numerical Study of Advanced Compression Ignition and Combustion in a Gasoline Direct Injection Engine," in *Proceedings of the ASME-ICEF 2019*, 2019.

[16] A. Shah, D. Kang, S. Goldsborough and T. Rockstroh, "Utilizing Static Autoignition Measurements to Estimate Intake Air Condition Requirements for Compression Ignition in a Multi-Mode Engine - Engine and RCM Experimental Study," in *SAE Technical Paper 2019-01-0957*, 2019.

[17] C. Kolodziez, M. Oamminger, S. J., T. Wallner, S. Wagnon and W. Pitz, "Effects of Fuel Laminar Flame Speed Compared to Engine Tumble Ratio, Ignition Energy, and Injection Strategy on Lean and EGR Dilute Spark Ignition Combustion," *SAE Int. J. Fuels Lubr.,* vol. 10, no. 1, pp. 82-94, 2017.

[18] T. Wallner, J. Sevik, R. Scarcelli, B. Kaul and R. Wagner, "Effects of Ignition and Injection Perturbation under Lean and Dilute GDI Engine Operation," in *SAE Technical Paper 2015-01-1871*, 2015.

[19] K. Richards, P. Senecal and E. Pomraning, "CONVERGE 2.4," Convergent Science, 2018.

[20] A. Babajimopoulos, D. Assanis, D. Flowers, S. Aceves and R. Hessel, "A Fully Coupled Computational Fluid Dynamics and Multizone Model with Detailed Chemical Kinetics for the Simulation of Premixed Charge Compression Ignition Engines," *Int. J. Engine Res.,* vol. 6, no. 5, pp. 497-512, 2005.

[21] C. Xu, P. Pal, X. Ren, S. Som, M. Sjöberg, N. Dam, Y. Wu, T. Lu and M. McNenly, "Numerical Investigation of Fuel Property Effects on Mixed-Mode Combustion in a Spark-Ignition Engine," in *Proceedings of ASME ICEF2019-7265*, 2019.

[22] N. Peters, Turbulent Combustion, Cambridge University Press, 2000.

[23] J. Ewald and N. Peters, "A Level Set Based Flamelet Model for the Prediction of Combustion in Spark Ignition Engines," in *15th International Multidimensional Engineering Models User Group*, Detroit, MI, 2005.

[24] R. Reitz, "Modeling of Atomization Processes in High-Pressure Vaporizing Sprays," *Atomization and Sprays,* vol. 3, no. 4, pp. 309-337, 1987.

[25] A. Amsden, "KIVA-3V: A Block-Structured KIVA Program for Engines with Vertical or Canted Valves," Los Alamos National Laboratory Technical Report LA-13313-MS, 1997.

[26] R. McCormick, "Co-Optimization of Fuels & Engines: Properties of Co-Optima Research GAsolines," 2018.

[27] N. Dam, M. Sjöberg and S. Som, "Large-Eddy Simulations of Spray Variability Effects on Flow Variability in a Direct-Injection Spark-Ignition Engine Under Non-Combusting Operating Conditions," in *SAE Technical Paper 2018-01-0196*, 2018.

[28] M. Mehl, K. Zhang, S. Wagnon, G. Kukkadapu, C. Westbrook, W. Pitz, Y. Zhang, H. Curran, M. Al Rachidi, N. Atef and M. Sarathy, "A comprehensive detailed kinetic mechanism for the simulation of transportation fuels," in *10th U.S. National Combustion Meeting*, 2017.

[29] T. Lu and C. Law, "A Directed Relation Graph Method for Mechanism Reduction," *Proc. Combustion Inst.,* vol. 30, pp. 1333-1341, 2005.

[30] X. Zheng, T. Lu and C. Law, "Experimental Counterflow Ignition Temperatures and Reaction Mechanisms of 1,3-Butadiene," *Proc. Combust. Inst.,* vol. 31, pp. 367-375, 1007.

[31] M. Leguille, F. Ravet, J. Le Moine, E. Pomraning, K. Richards and P. K. Senecal, "Coupled Fluid-Solid Simulation for the Prediction of Gas-Exposed Surface Temperature Distribution in a SI Engine," in *SAE Technical Paper 2017-01-0669*, 2017.

[32] S. Kim, J. Kim, A. Shah, R. Scarcelli and T. Rockstroh, "Numerical Analysis of Fuel Impacts on Advanced Compression Ignition Strategies for Multi-Mode Internal Combustion Engines," in *SAE Technical Paper 2020-01-1124*, 2020.

[33] R. Scarcelli, K. Richards, E. Pomraning, P. K. Senecal, T. Wallner and J. Sevik, "Cycle-to-Cycle Variations in Multi-Cycle Engine RANS Simulations," in *SAE Technical Paper 2016-01-0593*, 2016.

[34] K. J. Richards, D. P. E. Probst, P. K. Senecal and R. Scarcelli, "The Observation of Cyclic Variation in Engine Simulations When Using RANS Turbulence Modeling," in *ASME ICEF2014-5605*, 2014.

[35] R. Scarcelli, T. Wallner, K. Richards, E. Pomraning and P. K. Senecal, "A Detailed Analysis of the Cycle-To-Cycle Variations Featured by RANS Engine Modeling," in *International Multidimensional Engine Modeling User's Group Meeting*, Detroit, MI, USA, 2016.

[36] B. Johansson, "Cycle to Cycle Variations in S.I. Engines - The Effects of Fluid Flow and Gas Composition in the Vicinity of the Spark Plug on Early Combustion," in *SAE Technical Paper 962084*, 1996.

[37] M. Rashidi, "The Nature of Cycle-by-Cycle Variation in the S.I. Engine From High Speed Photographs," *Combustion and Flame,* vol. 42, pp. 111-122, 1981.

[38] C. Chen, M. Ameen, H. Wei, C. Iyer, F. Ting, B. Vanderwege and S. Som, "LES Analysis on Cycle-to-Cycle Variation of Combustion Process in a DISI Engine," in *SAE Technical Paper 2019-01-0006*, 2019.

[39] J. Szybist and D. Splitter, "Pressure and temperature effects on fuels with varying octane sensitivity at high load in SI engines," *Combustion and Flame,* vol. 177, pp. 49-66, 2017.

[40] J. Szybist, S. Wagnon, D. Splitter, W. Pitz and M. Mehl, "The Reduced Effectiveness of EGR to Mitigate Knock at High Loads in Boosted SI Engines," *SAE Int. J. Engines,* vol. 10, no. 5, pp. 2305-2318, 2017.

[41] Z. Yue and S. Som, "Fuel property effects on knock propensity and thermal efficiency in a direct-injection spark-ignition engine," *Applied Energy,* p. in press, 2019.

[42] M. Sellnau, W. Moore, J. Sinnamon, K. Hoyer, M. Foster and H. Justed, "GDCI Multi-Cylinder Engine for High Fuel Efficiency and Low Emissions," *SAE Int. J. Engines,* vol. 8, no. 2, pp. 775-790, 2015.

[43] J. Chang, Y. Viollet, A. Amer and G. Kalghatgi, "Fuel Economy Potential of Partially Premixed Compression Ignition (PPCI) Combustion with Naphtha Fuel," in *SAE Technical Paper 2013-01-2701*, 2013.

[44] S. Ciatti, M. Johanson, B. Das Adhikary and R. Reitz, "Efficiency and Emissions performance of Multizone Stratified Compression Ignition Using Different Octane Fuels," in *SAE Technical Paper 2013-01-0263*, 2013.